ACCEPTED MANUSCRIPT

Application of magnetite nanoparticle-modified walnut shell as an adsorbent for the removal of the organic dye Coomassie Brilliant Blue R-250

MOZHGAN BIUKI, HASSAN ZAVVAR MOUSAVI*, MAJID ARVAND AND HADI FALLAH MOAFI

Faculty of Chemistry, Department of Analytical Chemistry, University of Guilan, Rasht, Iran.

Abstract: In this research, a magnetic nanocomposite, walnut shell@Fe_3O_4, was synthesized as a natural adsorbent for the removal of Coomassie Brilliant Blue (CBB) R-250 organic dye from aqueous solutions, achieving a remarkable removal efficiency of 96.16%. The morphology of the nanocomposite was characterized using SEM and FTIR, revealing particle sizes of less than 18 nanometers. Additionally, BET analysis was performed, indicating a high surface area that enhances adsorption capacity. The influential variables affecting dye removal, including solution pH, stirring time, adsorbent dosage, initial dye concentration, temperature, and ionic strength, were optimized. The adsorption process was analyzed using Langmuir, Freundlich, Temkin, and Dubinin-Radushkevich isotherm models. The experimental results indicated that the process followed the Freundlich and Temkin isotherm models, suggesting the heterogeneous nature of the adsorbent surface. The kinetic conditions of adsorption were investigated using pseudo-first order and pseudo-second-order models, with results showing that the adsorption process of CBB followed the pseudo-second-order kinetic model, indicating the chemical adsorption of the dye onto the magnetic nanoparticles. Thermodynamic studies also revealed the spontaneous nature of the adsorption process, with a positive slope of the Van't Hoff curve indicating an exothermic reaction. Due to the equilibrium time of 5 minutes in the adsorption mechanism, the synthesized magnetic nanocomposite demonstrated a high CBB dye removal rate, making it suitable for treating dye-containing solutions.

Keywords: adsorption; thermodynamic; kinetic; magnetic nanocomposite; isotherm.

INTRODUCTION

Nowadays, water pollution has become one of the major issues. Various pollutants, including heavy metals, dyes, radioactive compounds, and organic and inorganic substances, contribute to water pollution.[1] Dyes, due to their wide applications in various industries, can be considered major pollutants in industrial effluents. They can lead to reduced photosynthetic activity in aquatic plants due to decreased light penetration in polluted waters,[2] increased biochemical oxygen demand, the generation of unpleasant odors, and the release of toxic substances.[3] Wastewater containing dyes is challenging to treat, as dyes are highly resistant to digestion and stable against oxidizing agents. Today, experts have realized that surface adsorption using cost-effective adsorbents is a good and economical method for wastewater treatment from dye compounds.[4] Surface adsorption using metallic nanoparticles has emerged as an environmentally friendly technology in recent years and has been investigated as an effective means for eliminating biological pollution in wastewater.[5] Multiple studies have been conducted in the field of removing Coomassie Brilliant Blue R-250 dye, including the use of raw oyster shell for the removal of Coomassie Brilliant Blue R-250 dye from aqueous solutions.[6] Poly(phenylene diamine)-grafted electrospun carbon nanofibers were effectively utilized for the adsorption of CBB dye.[7] starch/poly(alginic acid-cl-acrylamide) nanohydrogels demonstrated significant efficiency in removing Coomassie Brilliant Blue R-250.[8] Alginate-chitosan nanoparticles showed high adsorption capabilities for CBB.[9] The synthesis of a hybrid structured magnetite crosslinked polyionic liquid was explored for efficient Coomassie Brilliant Blue R-250 dye removal.[10] Modification of magnetite nanoparticles' surfaces with multifunctional ionic liquids for coomassie brilliant blue R-250 dye removal.[11] α-Chitin nanoparticles were used for the adsorption of Coomassie Brilliant Blue R-250 dye.[12] response surface methodology was applied for the removal of Coomassie blue dye using natural and acid-treated clays.[13] well-crystalline ZnO nanostructures were investigated for the removal of hazardous dyes, including CBB.[14] decolorization of Coomassie Brilliant Blue R-250 by dextran aldehyde-modified horseradish peroxidase.[15] adsorption of Coomassie brilliant blue R-250 dye onto novel activated carbon prepared from Nigella sativa L.[16] Magnetic nanoparticles refer to particles with an independent nature and maximum dimensions of around 100 nm that possess magnetic elements.[17] Among magnetic nanoparticles, iron nanoparticles, especially superparamagnetic Fe_3O_4 nanoparticles (magnetite), have received the most attention due to their abundance, low cost, non-toxicity, rapid response, good biocompatibility, lack of residual magnetism after removal of the external magnetic field, and high efficiency in adsorbing pollutants from contaminated water.[18]

The study aims to synthesize a magnetic nanocomposite using walnut shell and evaluate its effectiveness in removing CBB organic dye from water. Walnut
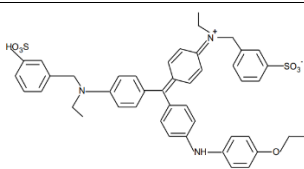
shell is chosen as the adsorbent due to its abundant availability, low cost, and high adsorption capacity. Interestingly, no previous research has explored the use of magnetic nanocomposites derived from walnut shell for CBB dye removal in aqueous solutions.

EXPERIMENTAL

Materials and methods

Iron (III) chloride hexahydrate ($FeCl_3 \cdot 6H_2O$, 99.9%), Iron (II) chloride tetrahydrate ($FeCl_2 \cdot 4H_2O$, 99.9%), ammonium hydroxide (NH_4OH, 25%), hydrochloric acid (HCl, 37%), sodium hydroxide (NaOH, 99%), acetic acid (CH_3COOH, 100%), nitric acid (HNO_3, 65%), and sulfuric acid (H_2SO_4, 98%) were all obtained from Merck and used in the experiment. The walnut shells were collected from mountainous areas near Rudbar; distilled water was used; and Coomassie Brilliant Blue R-250 dye ($C_{45}H_{44}N_3NaO_7S_2$) was employed. Silica gel with a mesh size of 60 (equivalent to a pore diameter of 0.0098 inches), a magnetic iron remover with a strength of 1.4 Tesla, a dual-beam UV-Vis spectrophotometer (JONIOR Model 35, Perkin-Elmer, USA, Texas), a pH meter (MTT65 model, Iran), mechanical and magnetic stirrers (TM52E model, Fan Azin Gostar, Iran), a digital scale with a precision of 0.0001 grams (AS220.R2 model, Radwag, Poland), an oven (Memmert, Germany), a centrifuge (D-7200 model, Hettich Universal, Germany), a scanning electron microscope (SEM) (MIRA3 model, Tescan, Czech Republic), a Fourier-transform infrared spectroscopy (FT-IR) instrument (Vertex70 model, Bruker, Germany), and a Brunauer–Emmett–Teller (BET) surface area analyzer (Autosorb iQ, Quantachrome Instruments) were used in this study. Additionally, laboratory equipment such as porcelain mortars and glassware like beakers, test tubes, and vials were utilized. The specifications of CBB organic dye are presented in Table I.

Table I. Characteristics of CBB R-250 Organic Dye

Chemical structure	
Dye type	Anionic
Chemical formula	$C_{45}H_{44}N_3NaO_7S_2$
Molecular weight (g mol^{-1})	825.97
Maximum absorption wavelength (nm)	555

Preparation of walnut shell

First, the walnut shells were dried after being collected by exposing them to direct sunlight. The walnut shells were initially washed with milk and then rinsed with distilled water. They were then placed in an oven at a temperature of 60 degrees Celsius for 24 hours to ensure complete drying. Once dried, the shells were placed in a mortar and ground into fine particles. Subsequently, these particles were washed multiple times with distilled water until they lost their original color. Next, 0.5 grams of the desired adsorbent were mixed with 0.5 M solutions of nitric acid, sulfuric acid, hydrochloric acid, acetic acid, and sodium hydroxide. The mixture was stirred on a magnetic stirrer at a speed of 400 rpm for 24 hours. The mixture was then

filtered, and any excess acid or base was removed by washing with distilled water multiple times. The adsorbent was dried in an oven at 60 degrees Celsius (overnight). The particles were then passed through a 60-mesh sieve to obtain uniform particles with a diameter less than 250 microns. To modify the surface of these particles and impart magnetic properties for ease of separation, magnetite nanoparticles were used through a chemical deposition method.[19]

Synthesis of walnut shell magnetic nanocomposite

The magnetic nanocomposite of walnut shell was synthesized using a co-precipitation method with iron (III) and iron (II) chlorides at a molar ratio of 2:1.[20] According to this method, 4.24 grams of $FeCl_3 \cdot 6H_2O$ and 1.55 grams of $FeCl_2 \cdot 4H_2O$ were dissolved in 100 milliliters of deionized water inside a flask. The resulting solution was placed under a nitrogen atmosphere for 20 minutes to remove dissolved oxygen and prevent oxidation. To obtain a homogeneous solution, the mixture was mechanically stirred using a magnetic stirrer. Next, the solution was heated to 80 degrees Celsius, and then 25% ammonium hydroxide was added dropwise over a period of 30 minutes to raise the pH of the solution to 11. Subsequently, 10 grams of prepared walnut shell, obtained in the previous step, were added to the suspension mixture. The reaction continued for 30 minutes with vigorous stirring. Finally, the magnetic composite was separated using a magnet and washed multiple times with distilled water through repeated distillation. In the final step, the magnetic composite was placed in an oven at 70 degrees Celsius for 4 hours to dry. The synthesized adsorbent was then ready for use in subsequent stages.[19]

RESULTS AND DISCUSSION

The morphology of walnut shell@Fe₃O₄ nanocomposite was investigated using scanning electron microscopy (SEM).

The morphology and particle size of the walnut shell@Fe_3O_4 nanocomposite were thoroughly analyzed using a scanning electron microscope (SEM). Fig. 1a presents the SEM image of the walnut shell prior to the deposition of magnetite nanoparticles, illustrating the natural structure and texture of the shells. In contrast, Fig. 1b displays the SEM image after the deposition of magnetite nanoparticles, revealing significant changes in morphology. The SEM images indicate a satisfactory size distribution of the magnetite particles, which are uniformly distributed across the walnut shell surface. The analysis shows that the average size of the magnetite particles is below 18 nanometers, suggesting the successful synthesis of nanoparticles with desirable dimensions for effective adsorption applications. The presence of numerous globules can be observed, indicating a high degree of aggregation and interaction among the magnetite nanoparticles.[21] This fine particle size is advantageous as it enhances the surface area available for adsorption processes, thereby improving the efficacy of the walnut shell @Fe_3O_4 nanocomposite in removing contaminants from aqueous solutions. Overall, the SEM characterization confirms that the walnut shell@Fe_3O_4 nanocomposite has been effectively synthesized with appropriate morphological properties for its intended applications.
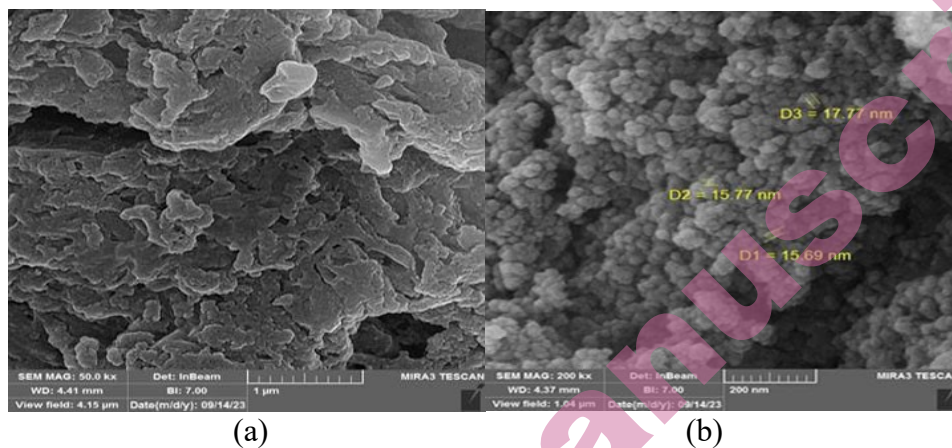
Fig 1. SEM images of the walnut shell surface (a) before and (b) after magnetite nanoparticle deposition

BET analysis

To determine the adsorbent's surface area, pore volume, and particle diameter, a BET analysis was conducted on 0.3545 grams of walnut shell@Fe$_3$O$_4$ at a temperature of 77 Kelvin using nitrogen gas (N$_2$). The specific surface area of the adsorbent was determined to be 12.311 m^2 g^{-1}, indicating a significantly higher potential for pollutant adsorption compared to many conventional adsorbents. A larger surface area plays a crucial role in adsorption capacity, depending on the type of pollutant. The results are presented in Table II.

The pore volume was measured at 0.055 cm^3 g^{-1}, and the average pore diameter was found to be 17.918 nm. This diameter exceeds that of many common pollutants, making it easier for pollutant molecules to enter the adsorbent's mesostructure. The examination revealed that the material exhibits mesoporous attributes, consistent with IUPAC criteria.[22] The combination of a high specific surface area, appropriate pore volume, and suitable pore diameter makes this adsorbent a promising option for environmental applications. Additionally, the surface of lignocellulose-based adsorbents like walnut shell is rich in various functional groups, enhancing the overall adsorption capacity for charged dye molecules.

Table II. Physical properties of walnut shell@Fe$_3$O$_4$

Parameter	Surface Area / m^2 g^{-1}	Pore Volume / cm^3 g^{-1}	Average Pore Diameter / nm
Value	12.311	0.055	17.918

Identification of the nanostructure of walnut shell@Fe$_3$O$_4$ using Fourier transform infrared (FTIR) spectroscopy

For a more detailed study of the nanostructure of the synthesized magnetic walnut shell nanoparticles, Fourier transform infrared (FTIR) spectroscopy was utilized. The FTIR spectrum of the synthesized nanoparticles is presented in Fig. 2. In this spectrum, the absorption band at 580 cm^{-1} corresponds to the stretching vibration of the Fe-O bond. The absorption bands at 655 cm^{-1} and 995 cm^{-1} are attributed to the bending vibrations of the C-H bonds. The absorption band at 1380 cm^{-1} represents the bending vibrations of the CH$_2$ group. while the absorption band at 1718 cm^{-1} corresponds to the C=O bond. and the absorption band at 3155 cm^{-1} represents the stretching vibration of the O-H bond.[19] Based on the infrared spectrum; it can be concluded that the magnetic nanocomposite of walnut shell has been successfully synthesized.
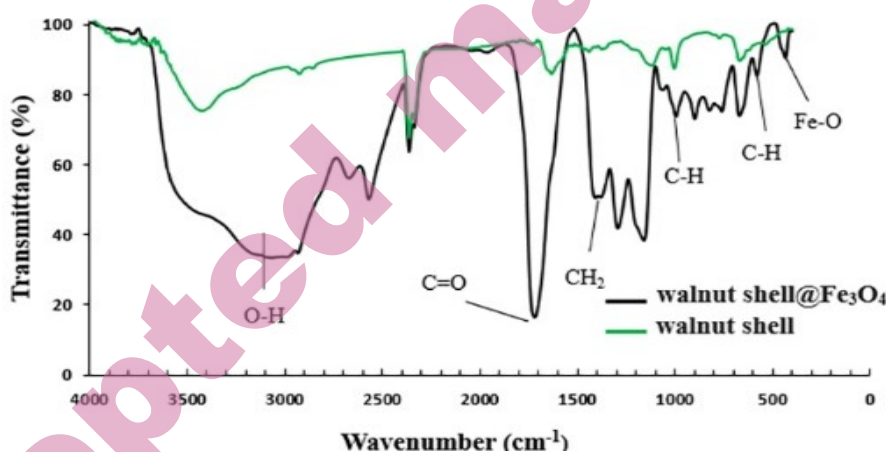

Fig. 2. FT-IR spectrum of walnut shell before and after nano-magnetite.

The zero point of charge (pH$_{PZC}$) of the walnut shell@Fe$_3$O$_4$ nanostructure

The zero point of charge (pH $_{PZC}$) refers to the pH at which the net surface charge of an adsorbent becomes zero. Determining this point is important for characterizing the surface properties of the adsorbent. Above the pH $_{PZC}$, the surface of the adsorbent becomes negatively charged, making it easier to adsorb ions with opposite charges (positively charged ions). Similarly, below the pH $_{PZC}$, the surface charge of the adsorbent becomes positive, leading to faster adsorption of negatively charged ions. 11 In this study, the effect of pH on the magnetic walnut shell nanocomposite was investigated. Solutions with different pH values ranging from 2 to 12 were prepared using sodium hydroxide (NaOH) and hydrochloric acid (HCl). The magnetic nanocomposites were added to each solution and stirred for 24 hours. After centrifugation, the final pH of each solution

was measured.[23] By plotting Fig. 3, the final pH against the initial pH, the zero point of charge (pH $_{PZC}$) of the nanocomposite was determined to be 6.
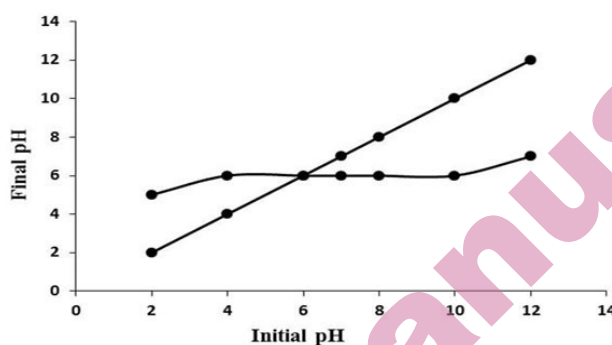

Fig 3. Zero point of charge diagram.

Adsorption experiments

The desired solutions were prepared using a dilution process from a stock solution. Then, adsorption experiments were conducted to investigate the effects of pH, contact time, adsorbent amount, initial dye concentration, temperature, and ionic strength on the adsorption of CBB by the magnetic walnut shell nanocomposite. Solutions of CBB were prepared in 25mL volumes, changing one of the factors influencing adsorption while keeping the other parameters constant to determine the optimal values. After preparing the solutions, each was stirred with a magnet and a magnetic stirrer at a constant speed (400 rpm). They were then separated using a centrifuge, and their adsorption was measured using a spectrophotometer at a maximum wavelength of 555 nm. The percentage removal and the amount of unabsorbed dye on the nanoparticles were calculated using Equations 1 and 2.

$$\text{Removal\%} = \frac{c_i - c_f}{c_i} \times 100 \quad (1)$$

$$q_e = \frac{(c_i - c_f) \times V}{w} \quad (2)$$

In the above equations, C_i / mg L^{-1} represents the initial concentration, and C_e / mg L^{-1} represents the unadsorbed or equilibrium concentration. Additionally, q_e / mg g^{-1} represents the adsorption capacity at equilibrium, V / L represents the volume of the solution, and w / g represents the amount of adsorbent.

Effect of pH

The pH of the solution affects the adsorption of CBB dye on the adsorbent surface. It changes the surface charge and influences the ionization state of the dye.[24] This affects the kinetics and equilibrium properties of the adsorption process. At an acidic pH, H$^+$ ions adsorb on the nanocomposite surface, giving

active groups a partial positive charge and making them more prone to binding the anionic dye, CBB. In this study, CBB dye solutions with a concentration of 50 mg L^{-1} were prepared at different pH values (2–12). The adsorption process was carried out by mixing the solutions with the adsorbent for 30 minutes and then measuring the adsorption using a spectrophotometer after centrifugation. The results showed that the adsorption percentage increased as the pH decreased. At lower pH values, the adsorbent surface acquired a positive charge, enhancing the interaction with the negatively charged dye molecules. Conversely, at higher pH values, the adsorption was less effective due to the presence of negative ions on the adsorbent surface.[25] pH 4 was identified as the optimal pH for further experiments (Fig. 4a).

Effect of contact time

Another significant factor influencing the adsorption process is contact time. For example, in a study, the most effective adsorbent was identified as the one that achieved the highest removal percentage in the shortest time.[26] In this study, the effect of contact time on the adsorption of CBB dye using a magnetic nanocomposite was examined. Solutions of CBB dye with a concentration of 50 mg L^{-1} were prepared at the optimal pH, and the adsorbent was added and stirred for different contact times. The results showed that the percentage of CBB removal increased with increasing contact time. However, after approximately 5 minutes, the removal percentage reached equilibrium, indicating minimal changes thereafter. This suggests that 5 minutes was identified as the optimal contact time for further investigations (Fig. 4b).

Effect of adsorbent dosage

In this study, the effect of adsorbent dosage on the adsorption process was investigated. Solutions of CBB dye with a concentration of 50 mg L^{-1} at the optimal pH were prepared, and different amounts of the magnetic nanocomposite adsorbent were added to each solution. The results showed that increasing the adsorbent dosage led to higher percentages of CBB dye removal. This can be attributed to the increased surface area and available binding sites provided by the higher adsorbent dosage.[27] The highest removal percentage was observed at an adsorbent dosage of 0.02 g, beyond which further increases in dosage had minimal impact. Therefore, an optimal adsorbent dosage of 0.02 g was determined for the magnetic nanocomposite (Fig. 4c).

Effect of initial dye concentration

The study investigated the impact of the initial concentration of CBB dye on the adsorption process. Solutions with varying concentrations (10-70 mg L^{-1}) were prepared under optimal conditions. After stirring and filtration, the adsorption data were analyzed. The results showed that as the initial dye concentration increased, the percentage of CBB removal gradually decreased. This is because higher

concentrations lead to more competition for the available adsorption sites on the adsorbent.[28] Therefore, the optimal initial concentration for CBB dye adsorption was determined to be 10 mg L⁻¹ (Fig. 4d).

Effect of temperature

The study examined the effect of temperature on the adsorption of CBB dye by a magnetic nanocomposite. Solutions with a volume of 25 mL and an initial concentration of 10 mg L⁻¹ of CBB dye were prepared under optimal pH conditions. The adsorption process was conducted at temperatures ranging from 273 to 308 kelvin with a stirring time of 5 minutes. The results revealed that as the temperature increased, the percentage of CBB removal by the adsorbent decreased. This indicates an exothermic adsorption process,[29] where higher temperatures reduce the adsorption capacity of the magnetic nanocomposite for CBB dye (Fig. 4e).

Effect of ionic strength

The study investigated the effect of ionic strength on the adsorption of CBB dye by a magnetic nanocomposite. Sodium chloride (NaCl) solutions with concentrations ranging from 0.1 to 1 M were prepared. The results showed that as the salt concentration increased, the removal efficiency of CBB dye by the nanocomposite decreased. This decrease in efficiency can be attributed to the formation of a protective layer on the surface of the adsorbent, which hinders the electrostatic interaction between the adsorbent and the dye molecules. The optimal condition for the experiment was determined to be zero ionic strength, without increasing the salt concentration[30] (Fig. 4f).

Equilibrium adsorption isotherms

The study aimed to analyze the adsorption data using different adsorption isotherms, namely Langmuir (equation 3), Freundlich (equation 4), Temkin (equation 5), and Dubinin-Radushkevich (equation 6) isotherms. These isotherms help in understanding the interaction mechanism between the adsorbate species and the adsorbent material.[31] Equilibrium adsorption isotherms are valuable for determining the distribution of absorbate molecules between the liquid and solid phases at equilibrium during the adsorption process.

$$\frac{C_e}{q_e} = \frac{1}{q_m b} + \frac{C_e}{q_m} \tag{3}$$

$$\ln q_e = \ln k_F + \frac{1}{n} \ln C_e \tag{4}$$

$$q_e = B_T \ln A_T + B_T \ln C_e \tag{5}$$

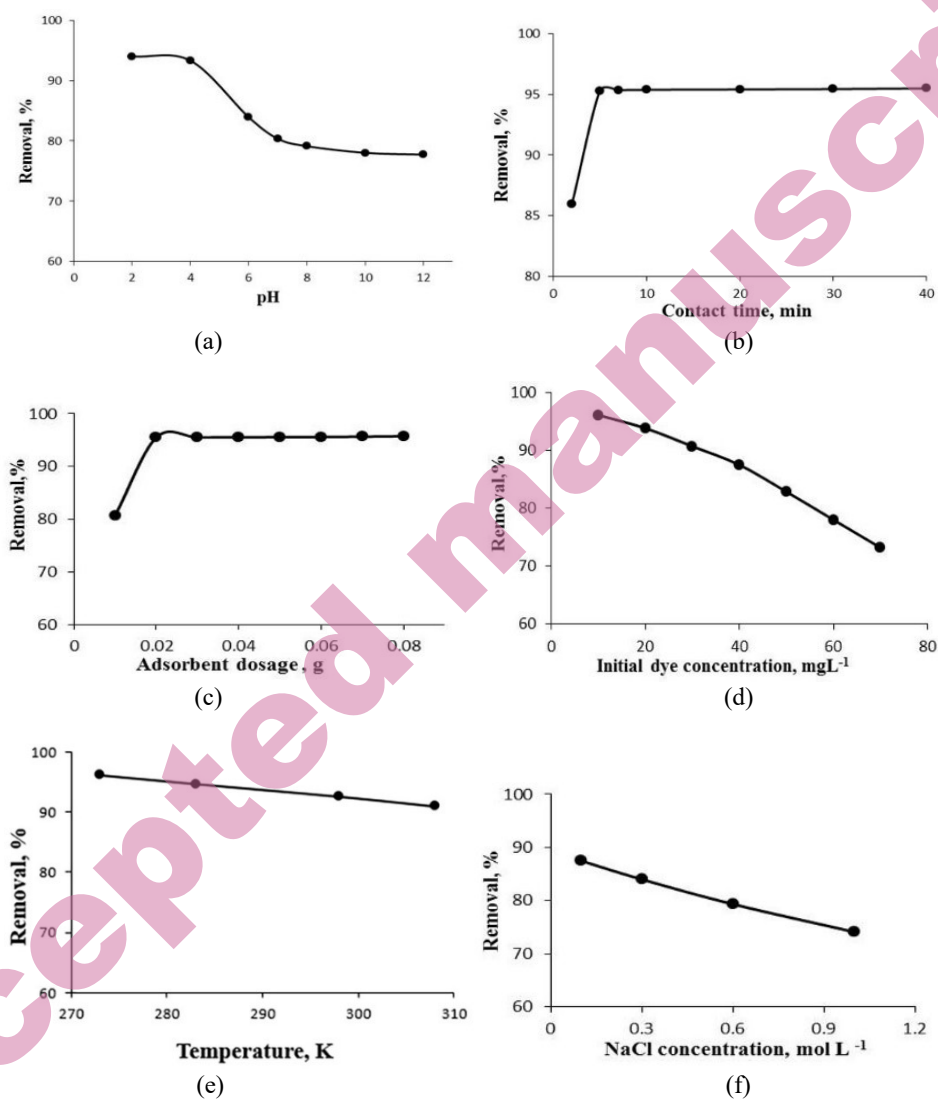$$\ln q_e = \ln q_m - \beta \varepsilon^2 \tag{6}$$

Fig 4. Effect of different (a) pH (b) contact time, (c) absorbent amount, (d) initial dye concentration, (e) temperature, (f) ion strength, on the adsorption of CBB by walnut shell magnetic nanocomposite.

In the above equations, C_e / mg L^{-1} represents the equilibrium concentration of the solution, q_e / mg g^{-1} denotes the adsorption capacity at equilibrium, q$_m$ / mg g^{-1} represents the maximum adsorption capacity, b / L mg^{-1} stands for the Langmuir constant, k_F / (mg g^{-1}) (L mg^{-1}) $^{(1/n)}$ represents the Freundlich constant where $1/n$ is the heterogeneity factor indicating the nature of the desired adsorption process. B_T / L mol^{-1} and A_T / L g^{-1} are the Temkin constants. β / mol^2 kJ^{-2} represents the useful

activity coefficient and ε / kJ mol^{-1} is the Polanyi potential. The linear plots for the Langmuir, Freundlich, Temkin, and Dubinin-Radushkevich equations are obtained by plotting C_e/q_e against C_e, $\ln q_e$ against $\ln C_e$, q_e against $\ln C_e$, and $\ln q_e$ against ε^2, respectively.[32]

Based on the results presented in Table III and the correlation coefficients (R^2) obtained for the different models, it can be concluded that the adsorption data in this study for the walnut shell magnetic nanocomposite follows the Freundlich and Temkin isotherms. This suggests that the adsorption process occurs heterogeneously and involves multiple layers. The maximum monolayer surface adsorption capacity of the magnetic nanocomposite, as determined from the Langmuir isotherm, is observed to be 212.76 mg g^{-1}. Moreover, the equilibrium parameter value (R_L) ranging from 0 to 1 and the intensity of adsorption (n) ranging from 1 to 10 indicate favorable adsorption using this adsorbent.[33]

Table III. The values of constants and correlation coefficients related to Langmuir, Freundlich, Temkin, and Dubinin-Radushkevich (D-R) equilibrium adsorption isotherms for the adsorption of CBB.

Langmuir	Freundlich	Temkin	Dubinin-Radushkevich
$R^2 = 0.9505$	$R^2 = 0.9907$	$R^2 = 0.9917$	$R^2 = 0.9342$
$q_m = 212.76$	$n = 1.23$	$B_T = 33.48$	$q_m = 65.72$
$b = 0.037$	$k_F = 8.94$	$A_T = 0.57$	$\beta = 2.52$
$R_L = 0.34$			

Adsorption kinetics

To gain a better understanding of the surface adsorption process, it is important to study the kinetics of the adsorption. The kinetics of adsorption provide insights into the efficiency of the adsorption process and the stages involved, such as film diffusion, intraparticle diffusion, surface diffusion, or a combination of these stages. In this study, two kinetic models were employed to determine the better fit: the pseudo-first-order Lagergren model (equation 8) and the pseudo-second-order Ho model (equation 9). The kinetic parameters obtained from these models are presented in Table IV.

$$\frac{dq}{dt} = k_1(q_e - q_t) \quad (7)$$

In equation 7, q_e / mg g^{-1} and q_t / mg g^{-1} represent the adsorption capacities at equilibrium and time t, respectively. k_1 / min^{-1} is the rate constant for surface adsorption in thepseudo-first-order kinetic model. By taking the natural logarithm of both sides of equation 7, another form of the pseudo-first-order kinetic equation is obtained, known as the Lagergren equation.

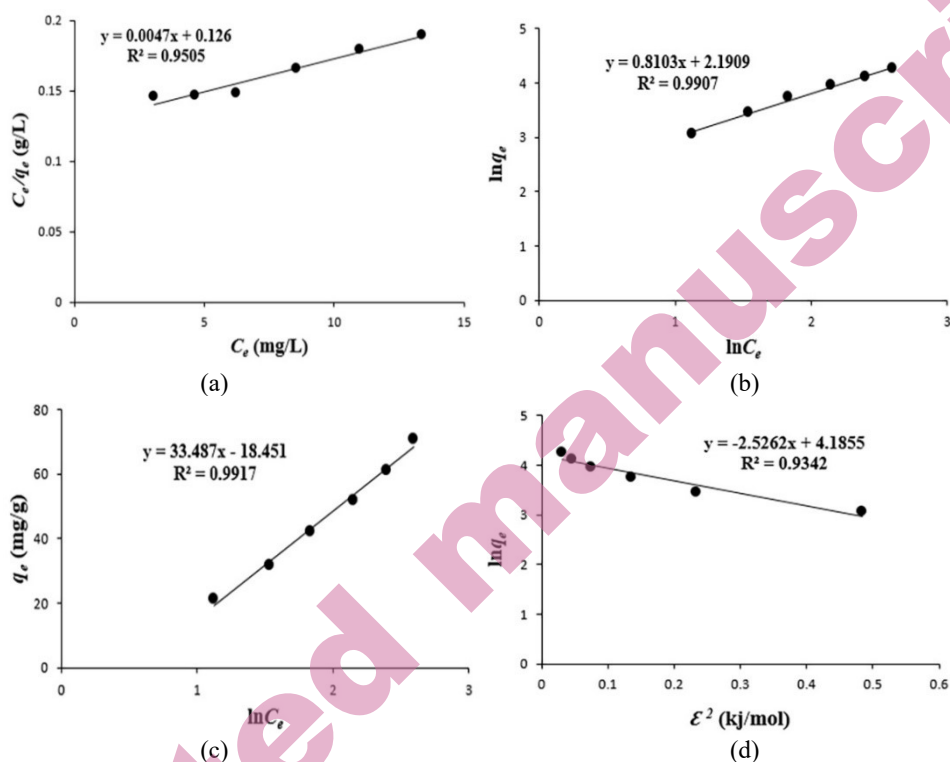$$ln(q_e - q_t) = ln\, q_{e1} - k_1 t \quad (8)$$

Fig 5. Graphs related to equilibrium adsorption isotherms: a) Langmuir, b) Freundlich, c) Temkin, and d) Dubinin-Radushkevich for the adsorption of CBB.

In that equation, q_{e1} represents the adsorption capacity obtained based on the pseudo-first-order kinetic model. By plotting a linear graph of $ln(q_e - q_t)$ against t and analyzing the slope and intercept, the values of k_1 and q_{e1} can be determined. The pseudo-second-order kinetic equation, based on the adsorption capacity, is presented as follows:

$$\frac{dq}{dt} = k_2(q_e - q_t)^2 \tag{9}$$

In this equation, k_2 / g (mg min)$^{-1}$ represents the rate constant for the pseudo-second-order kinetic equation. By integrating and rearranging this equation, another form of the equation can be obtained, as follows:

$$\frac{t}{q_t} = \frac{1}{k_2 q_{e2}^2} + \frac{t}{q_{e2}} \tag{10}$$

In the above equation, q_{e2} / mg g^{-1} represents the adsorption capacity obtained based on the pseudo-second-order kinetic model. By plotting the graph of t/q_t against t and analyzing the slope and intercept, the adsorption capacity at equilibrium (q_{e2}) and the pseudo-second-order rate constant (k_2) can be calculated. [34, 35] Based on the coefficient of determination (R^2) obtained, if the pseudo-second-

order kinetic model has a higher R^2 value compared to the pseudo-first-order kinetic model, it can be concluded that the adsorption process in this study follows pseudo-second-order kinetics. Furthermore, the nature of adsorption is considered to be chemical in nature.[36]

Table IV. Pseudo-first order and pseudo-second order kinetic parameters by walnut shell magnetic nanocomposite.

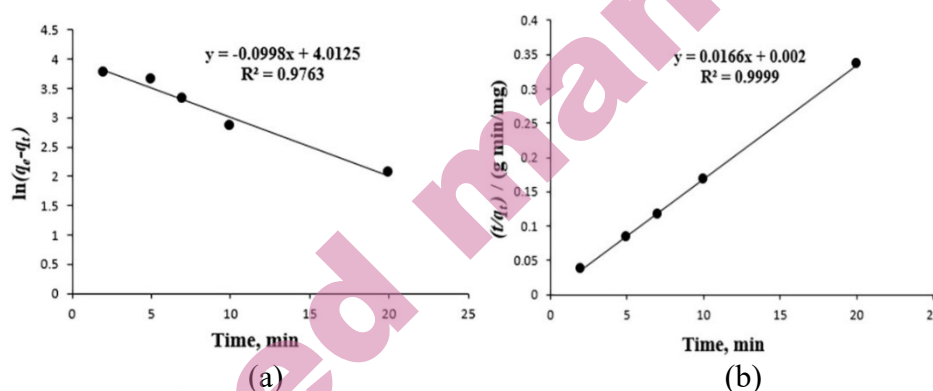| Pseudo-first-order model			Pseudo-second-order model		
K_1 / min^{-1}	q_e / mg g^{-1}	R^2	K_2 / g mg^{-1} min^{-1}	q_{e2} / mg g^{-1}	R^2
0.099	55.28	0.9763	0.13	60.24	0.9999

Fig 6. Kinetic graphs a) pseudo-first order and b) pseudo-second order for the adsorption of CBB.

Adsorption Thermodynamics

In this study, the changes in adsorption capacity with respect to temperature were examined to determine the nature of the adsorption process (exothermic or endothermic). The optimal temperature for maximum adsorption and desorption was identified. Adsorption constants and equilibrium constants were calculated based on the slope of the curves. Lower temperatures were found to be more economically favorable for the adsorption process. Thermodynamically, a negative change in Gibbs free energy ($\Delta G°$) indicates spontaneous adsorption. A negative standard enthalpy change ($\Delta H°$) suggests an exothermic adsorption process. Changes in standard entropy ($\Delta S°$) indicate changes in system entropy.[37] For significant adsorption, the change in Gibbs free energy should be negative. The change in Gibbs free energy of adsorption is defined as follows:

$$\Delta G^o = -RT \ ln K_c \qquad (11)$$

In that equation, T / K is the temperature, R / 8.314 kJ mol^{-1}K^{-1} is the universal gas constant, and K_c / mg L^{-1} is the equilibrium constant of adsorption. The relationship is expressed as follows:

$$K_c = \frac{q_e}{c_e} \tag{12}$$

In that equation, q_e / mg L^{-1} represents the equilibrium concentration of the adsorbate species on the adsorbent, and C_e / mg L^{-1} represents the equilibrium concentration of the adsorbate species in the solution. Other thermodynamic variables, such as the change in Gibbs free energy, the change in enthalpy, and the standard entropy change of adsorption, can be obtained using the following equation:

$$\Delta G^o = \Delta H^o - T\Delta S^o \tag{13}$$

Thermodynamic parameters such as the changes in enthalpy ($\Delta H°$) and entropy ($\Delta S°$) can also be obtained from the Van't Hoff equation:

$$ln\,K_c = \frac{\Delta S^o}{R} - \frac{\Delta H^o}{RT} \tag{14}$$

By plotting ln K_c against $1/T$ and determining the slope and intercept from the origin of the resulting curve, the variables $\Delta H°$ and $\Delta S°$ can be obtained.[38, 39] In this study, thermodynamic parameters of adsorption such as the changes in Gibbs free energy ($\Delta G°$), enthalpy ($\Delta H°$), and entropy ($\Delta S°$) related to the equilibrium constants of adsorption were obtained using equations (11) to (14). The results are presented in Table V.

According to Table V, the changes in Gibbs free energy ($\Delta G°$) for the dye CBB in this study are negative. Therefore, it can be concluded that the adsorption process by the magnetic walnut shell nanocomposite occurs spontaneously. The negative value of the changes in enthalpy ($\Delta H°$) indicates that the adsorption process is exothermic and serves as a favorable factor in this process. The negative value of the changes in entropy ($\Delta S°$) indicates a decrease in disorder within the system, suggesting that at higher temperatures, the adsorbent will have reduced adsorption capacity.[40]

Table V. Thermodynamic parameters of the adsorption process of CBB dye by magnetic nanocomposite at different temperatures

T / K	K_c / mg L^{-1}	$\Delta G°$/ KJ mol^{-1}	$\Delta H°$/ KJ mol^{-1}	$\Delta S°$ / kJ mol^{-1}K^{-1}	R^2
273	5.26	-3.77			
283	3.47	-2.92	-24.42	-0.075	0.9991
298	2.13	-1.87			
308	1.52	-1.08			

Table VI. Impact of Temperature on the Removal Efficiency of CBB

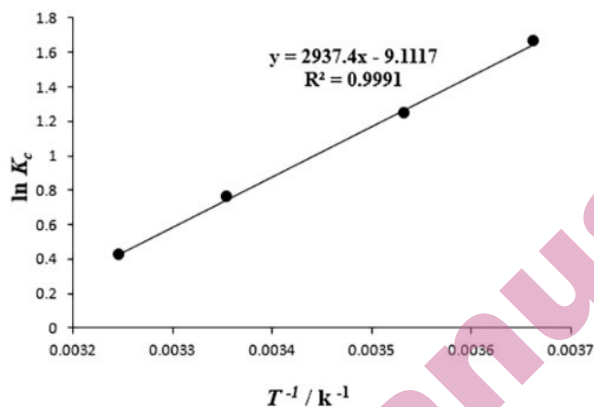| T / K	q_{exp}/ mg g^{-1}	Removal, %
273	10.10	96.16
283	9.19	94.70
298	7.87	92.60
308	6.87	91.00

Fig 7. Thermodynamic graph versus temperature in Kelvin for CBB.

Comparison study

In Table VII, a detailed comparison of the maximum adsorption capacity of various adsorbents for the removal of CBB dye is presented. According to Table VII, it can be concluded that the magnetic walnut shell nanocomposite (walnut shell@Fe$_3$O$_4$) has achieved a suitable maximum adsorption capacity compared to other adsorbents, indicating that this adsorbent is effective for the removal of CBB from aqueous solutions.

Table VII. Comparison of proposed adsorbent with some adsorbents used for CBB removal

Adsorbent	q_{max} / mg g^{-1}	Refrence
Natural agalmatolite	11.29	[13]
Natural kaolinite	22.89	[13]
Starch/poly(alginic acid-cl-acrylamide) nanohydrogel	31.24	[8]
p-ECNFs	141.00	[7]
o-ECNFs	107.80	[7]
m-ECNFs	46.90	[7]
Activated carbon (Nigella sativa L)	14.49	[16]
α-Chitin nanoparticles	8.55	[12]
walnut shell@Fe$_3$O$_4$	212.76	This study

CONCLUSION

In this study, a simple and effective method was used in this study to remove CBB dye from water using walnut shell modified with magnetic nanoparticles. The walnut shell was chemically coated with magnetite nanoparticles, creating a magnetic walnut shell nanocomposite. The results showed that this modified adsorbent has great potential for CBB dye removal. The removal percentage decreased with increasing dye concentration and decreasing adsorbent dosage. Isotherm studies confirmed multilayer adsorption on the adsorbent's heterogeneous surfaces, with a maximum adsorption capacity of 212.76 mg g^{-1} at the optimal dye

concentration. Kinetic studies indicated chemical adsorption on the adsorbent's surface. Thermodynamic investigations revealed that the adsorption process was spontaneous, and the Van't Hoff curve showed an exothermic nature of the dye adsorption on the synthesized adsorbent.

И З В О Д

ПРИМЕНА МОДИФИКОВАНЕ ЉУСКЕ ОРАХА НАНОЧЕСТИЦАМА МАГНЕТИТА КАО АДСОРБЕНСА ЗА УКЛАЊАЊЕ ОРГАНСКЕ БОЈЕ COOMASSIE BRILLIANT BLUE R-250

MOZHGAN BIUKI, HASSAN ZAVVAR MOUSAVI, MAJID ARVAND AND HADI FALLAH MOAFI

Faculty of Chemistry, Department of Analytical Chemistry, University of Guilan, Rasht, Iran.

Магнетни нанокомпозит, љуска ораха@Fe$_3$O$_4$, синтетисан је као природни адсорбенс за уклањање органске боје Coomassie Brilliant Blue (CBB) R-250 из водених раствора, са ефикасношћу од 96,16%. Морфологија нанокомпозита је окарактерисана коришћењем SEM и FTIR, при чему је утврђена величине честица мања од 18 нанометара. Додатно, извршена је BET анализа која указује на велику површину која повећава капацитет адсорпције. Оптимизоване су варијабле које утичу на уклањање боје, и то: pH раствора време мешања, количина адсорбенса, почетна концентрација боје, температура и јонска сила. Проценс адсорпције је анализиран применом Langmuir, Freundlich, Temkin, and Dubinin-Radushkevich модела изотерми. Експериментални резултати су показали да процес адсорпцијепрати Freundlich и Temkin изотермне моделе што указује на хетерогену природу површине адсорбенса. Применом модела псеудо-првог и псеудо-другог реда су испитивани кинетички услови адсорпције. Резултати су показали да процес адсорпције CBB прати кинетички модел псеудо-другог реда што указује на хемијску адсорпцију боје на наночестицама. Термодинамичким студијама је утврђена спонтана природа процеса адсорпције, са позитивним нагибом Ван'т Хофове криве што указује на егзотермну реакцију. Због кратког времена успостављања равнотеже од 5 минута, синтетисани магнетни нанокомпозит је показао велику брзину уклањања CBB боје, што га чини погодним за третман раствора који садрже боје.

(Примљено 21. априла; ревидирано 10. октобра; прихваћено 17. новембра 2024.)

REFERENCES

1. R. Zein, H. Fathony, P. Ramadhani, Deswati, *J. Serb. Chem. Soc.* **89** (2024) 123 (https://doi.org/10.2298/JSC230303084Z)
2. M. Vukčević, M. Maletić, B. Pejić, N. Karić, K. Trivunac, A. Perić Grujić, *J. Serb. Chem. Soc.* **88** (2023) 669 (https://doi.org/10.2298/JSC221213015V)
3. Z. Y. Velkova, G. K. Kirova, M. S. Stoytcheva, V. Gochev, *J. Serb. Chem. Soc.* **83** (2018) 107 (https://doi.org/10.2298/JSC170519093V)
4. N. Nourbakhsh, H. Zavvar Mousavi, E. Kolvari, A. Khaligh, *Appl. Chem. Today.* **17** (2023) 33 (https://doi.org/10.22075/chem.2021.23896.1991)
5. M. Ghereghlou, A. A. Esmaeili, M. Darroudi, *Sep. Sci. Technol.* **57** (2022) 2005 (https://doi.org/10.1080/01496395.2022.2029490)

6. V. K. Veni, T. H. Brenda, *IOP Conf. Ser.: Earth Environ. Sci.* **765** (2021) 012039 (https://doi.org/10.1088/1755-1315/765/1/012039)

7. B. M. Thamer, A. Aldalbahi, M. Moydeen A, H. El-Hamshary, A. M. Al-Enizi, M. H. El-Newehy, *Mater. Chem. Phys.* **234** (2019) 133 (https://doi.org/10.1016/j.matchemphys.2019.05.087)

8. G. Sharma, M. Naushad, A. Kumar, S. Rana, S. Sharma, A. Bhatnagar, F. J. Stadler, A. A. Ghfar, M. R. Khan, *Process Saf. Environ. Prot.* **109** (2017) 301 (https://doi.org/10.1016/j.psep.2017.04.011)

9. J. A. Putri, A. Suratman, R. Roto, *J. Metastable Nanocrystall. Mater.* **34** (2022) 63 (https://doi.org/10.4028/v-4f958r)

10. A. O. Ezzat, A. M. Tawfeek, J. R. Rajabathar, H. A. Al-Lohedan, *Molecules* **27** (2022) 441 (https://www.mdpi.com/1420-3049/27/2/441)

11. A. O. Ezzat, A. M. Tawfeek, F. Mohammad, H. A. Al-Lohedan, *J. Mol. Liq.* **358** (2022) 119195 (https://doi.org/10.1016/j.molliq.2022.119195)

12. S. Dhananasekaran, R. Palanivel, S. Pappu, *J. Adv. Res.* **7** (2016) 113 (https://doi.org/10.1016/j.jare.2015.03.003)

13. P. F. de Sales, Z. M. Magriotis, M. A. L. S. Rossi, R. F. Resende, C. A. Nunes, *J. Environ. Manag.* **130** (2013) 417 (https://doi.org/10.1016/j.jenvman.2013.08.067)

14. G. R. Chaudhary, P. Saharan, A. Umar, S. K. Mehta, S. Mor, *Sci. Adv. Mater.* **5** (2013) 1886 (https://doi.org/10.1166/sam.2013.1701)

15. M. Altikatoglu, M. Celebi, *Artif. Cells Blood Substit. Biotechnol.* **39** (2011) 185 (https://doi.org/10.3109/10731199.2010.533124)

16. N. T. Abdel-GhANi, G. A. El-Chaghaby, E.-S. A. Rawash, E. C. Lima, *J. Chil. Chem. Soc.* **62** (2017) 3505 (https://doi.org/10.4067/S0717-97072017000200016)

17. S. Dehghan Abkenar, M. Hassannezhad, M. Hosseini, M. R. Ganjali, *J. Serb. Chem. Soc.* **84** (2019) 701 (https://doi.org/10.2298/JSC181228038D)

18. X.-S. Li, G.-T. Zhu, Y.-B. Luo, B.-F. Yuan, Y.-Q. Feng, *TrAC, Trends Anal. Chem.* **45** (2013) 233 (https://doi.org/10.1016/j.trac.2012.10.015)

19. M. Bordbar, N. Negahdar, B. Khodadadi, *J. Nanostruct.* **12** (2022) 262 (https://doi.org/10.22052/JNS.2022.02.005)

20. S. Rahnama, S. Shariati, F. Divsar, *Comb. Chem. High Through. Screen.* **21** (2018) 583 (https://doi.org/10.2174/1386207321666181019111211)

21. M. Khan, S. Naseer, M. Khan, R. Nazir, A. Badshah, Adnan, S. Shujah, A. Parveen, *Desal. Water Treat.* **228** (2021) 286 (https://doi.org/10.5004/dwt.2021.27352)

22. A. Ali Ahmed, Z. Hattab, Y. Berredjem, S. Hamoudi, R. Djellabi, *Desal. Water Treat.* **317** (2024) 100278 (https://doi.org/10.1016/j.dwt.2024.100278)

23. M. Erfani, R. Ansari, H. Zavvar Mousavi, *Appl. Chem. Today.* **17** (2022) 149 (https://doi.org/10.22075/chem.2022.23980.1994)

24. S. Temel, E. Yaman, N. Ozbay, F. O. Gokmen, *J. Serb. Chem. Soc.* **85** (2020) 939 (https://doi.org/10.2298/JSC190517114T)

25. D. Kosale, C. Thakur, V. K. Singh, *J. Serb. Chem. Soc.* **88** (2023) 653 (https://doi.org/10.2298/JSC220830021K)

26. S. Jadali, S. M. Sajjadi, H. Zavvar Mousavi, M. Rajabi, *Anal. Bioanal. Chem. Res.* **4** (2017) 171 (https://doi.org/10.22036/abcr.2016.67517.1122)

27. M. Hadnađev Kostić, T. Vulić, Đ. Karanović, M. Milanović, *J. Serb. Chem. Soc.* **87** (2022) 1011 (https://doi.org/10.2298/JSC220228034H)

28. Z. Lotfi, H. Z. Mousavi, S. M. Sajjadi, *Anal. Methods* **9** (2017) 4504 (https://doi.org/10.1039/C7AY01166K)

29. J. Rahchamani, H. Z. Mousavi, M. Behzad, *Desalination* **267** (2011) 256 (https://doi.org/10.1016/j.desal.2010.09.036)
30. S. M. Seyed Danesh, H. Faghihian, S. Shariati, *J. Nano Res.* **52** (2018) 54 (https://doi.org/10.4028/www.scientific.net/JNanoR.52.54)
31. Z. Dahaghin, H. Z. Mousavi, L. Boutorabi, *J. Mol. Liq.* **243** (2017) 380 (https://doi.org/10.1016/j.molliq.2017.08.018)
32. S. Eftekhari, M. R. Sohrabi, S. Mortazavinik, *Iran. J. Chem. Chem. Eng.* (2024) (https://doi.org/10.30492/ijcce.2024.2016928.6343)
33. D. Marković, S. Milovanović, M. Radoičić, Ž. Radovanović, I. Zizovic, Z. Šaponjić, M. Radetić, *J. Serb. Chem. Soc.* **83** (2018) 1379 (https://doi.org/10.2298/JSC180913089M)
34. C. A. P. Almeida, N. A. Debacher, A. J. Downs, L. Cottet, C. A. D. Mello, *J. Colloid Interface Sci.* **332** (2009) 46 (https://doi.org/10.1016/j.jcis.2008.12.012)
35. I. Espinoza, C. Sandoval Pauker, L. Ramos Guerrero, P. Vargas Jentzsch, F. Muñoz Bisesti, *J. Serb. Chem. Soc.* **85** (2020) 547 (https://doi.org/10.2298/JSC190804119E)
36. A. A. Fodeke, O. O. Olayera, *J. Serb. Chem. Soc.* **84** (2019) 1143 (https://doi.org/10.2298/JSC190209042F)
37. S. K. Hassaninejad-Darzi, H. Z. Mousavi, M. Ebrahimpour, *J. Mol. Liq.* **248** (2017) 990 (https://doi.org/10.1016/j.molliq.2017.10.126)
38. K. Gul, H. Khan, N. Muhammad, B. Ara, T. U. H. Zia, *Sep. Sci. Technol.* **56** (2021) 2507 (https://doi.org/10.1080/01496395.2020.1839498)
39. A. C. Enache, P. Samoila, C. Cojocaru, R. Apolzan, G. Predeanu, V. Harabagiu, *Sustainability* **15** (2023) 2704 (https://doi.org/10.3390/su15032704)
40. I. Badran, R. Khalaf, *Sep. Sci. Technol.* **55** (2020) 2433 (https://doi.org/10.1080/01496395.2019.1634731).